Journal of Molecular Liquids 405 (2024) 124909

Contents lists available at ScienceDirect

Journal of Molecular Liquids

journal homepage: www.elsevier.com/locate/molliq

On the molecular mechanisms of H_2/N_2 uptake in confined ionic liquids: A computational study

Martín Otero-Lema [a,b,1], Raúl Lois-Cuns [a,b,1], Pablo Martínez-Crespo [a,b], Alejandro Rivera-Pousa [a,b], Hadrián Montes-Campos [a,b,c,*], Trinidad Méndez-Morales [a,b,*], Luis M. Varela [a,b]

[a] Grupo de Nanomateriais, Fotónica e Materia Branda, Departamento de Física de Partículas, Universidade de Santiago de Compostela, Campus Vida s/n, Santiago de Compostela, E-15782, Galicia, Spain
[b] Instituto de Materiais (iMATUS), Universidade de Santiago de Compostela, Avenida do Mestre Mateo 25, Santiago de Compostela, E-15782, Galicia, Spain
[c] CIQUP, Institute of Molecular Sciences (IMS)-Departamento de Química e Bioquímica, Faculdade de Ciências da Universidade do Porto, Rua Campo Alegre, Porto, 4169-007, Portugal

ARTICLE INFO

Dataset link: https://doi.org/10.5281/zenodo.10495511

Keywords:
Carbon nanotubes
Ionic liquids
Molecular modelling
Gas uptake
Hydrogen
Nitrogen

ABSTRACT

Classical molecular dynamics and hybrid grand canonical Monte Carlo/molecular dynamics simulations were combined to analyze the gas uptake mechanism of hydrogen and nitrogen molecules inside carbon nanotubes filled with an ionic liquid. Several nanotube diameters (from 6 Å to 12.24 Å) and two different ionic liquids (ethylammonium nitrate and 1-ethyl-3-methylimidazolium tetrafluoroborate) were considered to study their effect on the gas capture capacity and on the location of gas molecules within the nanotubes. The simulations showed that nitrogen absorption ability is, in general, greater than that of hydrogen, with the aprotic ionic liquid being more efficient for gas confinement. In addition, gas capture was observed to increase from a scarce 0.4% in bulk ionic liquids up to 8%-25% inside small nanotubes, and the maximum gas uptake was observed for those nanotubes that allow for a greater degree of conformational freedom of the ionic liquid. However, our calculations show that, whereas hydrogen storage is mainly governed by the amount of accessible free volume, for understanding that of nitrogen solvation energetics must be also considered. In all cases, gas molecules are absorbed in the ionic liquid-rich-region, but the interactions with the other components of the system favour their accommodation closer to the carbon wall than to the nanotube centre. Finally, single-particle dynamics of gas molecules was analyzed by means of the velocity autocorrelation functions and the vibrational density of states, which show a blue-shifting when increasing the radius of the nanotube.

1. Introduction

With the growth of world population and the improvement of the living standards, the demand of energy is also increasing and leading to an urgent need of changing our energy production, distribution and consumption patterns to achieve greater sustainability. In this context of energy transition, several strategies have been followed to develop renewable energy technologies and achieve deep decarbonization at large scale and in the shortest timeframe possible. For example, carbon capture and storage is expected to be the key for mitigating carbon dioxide (CO_2) emissions and reverting the trend of the global climate temperature rise [1]. Green hydrogen (H_2) has also been identified as a potential game changer and the interest in mechanisms that enable its storage, transportation and use is reaching unprecedented levels. Not in vain, it can be used in fuel cell electric vehicles, manufacturing processes, electricity grid stabilization and green ammonia (NH_3) production [2]. The latter is a much more practical alternative to fossil fuels, as it can be produced and stored more easily than green hydrogen, but it also costs more [3].

In any case, the global urgency for the implementation of fossil fuel alternatives has made the storage of gases such as CO_2, H_2 and nitrogen (N_2) to be a major challenge for materials science. Over the last decades, solid porous materials such as zeolites [4,5], carbon-based materials [6], metal-organic frameworks (MOFs) [7,8] or covalent organic

* Corresponding authors.
E-mail addresses: hadrian.montes@usc.es (H. Montes-Campos), trinidad.mendez@usc.es (T. Méndez-Morales).
[1] Contributed equally to this work.

https://doi.org/10.1016/j.molliq.2024.124909
Received 2 February 2024; Received in revised form 19 April 2024; Accepted 2 May 2024
Available online 10 May 2024

frameworks (COFs) [9] have been reported as promising candidates for gas capture and storage, mainly due to their large accessible surface areas and functionalizable pore environments. Other technique that can also serve as a new cornerstone to support gas trapping and accumulation is the use of ionic liquids (ILs) [10–14], which are "green" solvents completely composed of ions with melting point below 100 °C [15]. These compounds have received intense attention due to their unique characteristics, which include nonvolatily and nonflammability, high thermal and chemical stability, biodegradability and, most important, the possibility to systematically tune their physical and chemical properties with several combinations of cations and anions [16–19]. Nevertheless, the two major drawbacks for their commercial application are their high viscosity, which leads to low adsorption and desorption rates, and elevated production cost. The search for new approaches to use ILs in a different way and overcome these issues has proposed their incorporation into porous materials, thus leading to the so-called supported ionic liquids (SILs) [20]. This strategy has potential advantages such as enhanced mechanical strength, decreased viscosity and the use of a lower amount of IL. In addition, it has been shown that this IL nanoconfinement into the pores of a solid support also increases gas absorption. For example, Harmanli et al. [21] observed experimentally a giant N_2 uptake, 10 times higher than in neat IL, in an IL confined in the pores of carbon materials. Many researchers have investigated several options to be used as ideal encapsulant materials for SILs, such as membranes [22–27], MOFs [28–35], zeolite imidazolate frameworks (ZIFs) [36–39], carbon-based materials [21,40–43] and mesoporous silica gels [44], through experimental and computational means. In this context, Wang et al. [23] investigated CO_2 solubility in ILs confined in hydrophobic and hydrophilic membranes, showing that it was a little higher in the last case and also higher than that in the bulk IL phase. Also experimentally, Ibrahim and coworkers [29] highlighted the importance of the choice of the IL ions, since CO_2 capture performance of 1-butyl-3-methylimidazolium acetate supported on MOFs exhibited almost double capacity than that of the pristine MOF, whereas 1-propyl-3-methylimidazolium bis(trifluoromethylsulfonyl)imide did not show any uptake enhancement.

All the aforementioned studies have shown that SILs can be regarded as potential candidates for gas capture and storage. However, most of them have focused on CO_2, and weakly interacting gases like H_2 or N_2 remained nearly unnoticed, despite several works having identified ILs as attractive electrolytes for the electrocatalytic reduction of N_2 to NH_3 [21,45,46]. Among the very few works reported up to now, Shi and Luebke [47] employed Monte Carlo (MC) and molecular dynamics (MD) simulations to compare the absorption and diffusivity of CO_2, N_2 and H_2 in 1-n-hexyl-3-methylimidazolium bis(trifluoromethylsulfonyl)amide confined in silica slit pores, obtaining larger values than in the bulk IL. Also by means of atomistic simulations, Shi and Sorescu [48] analyzed the effect of confining different amounts in the same IL inside carbon nanotubes (CNTs) with a radius of 6.102 Å and 13.56 Å upon CO_2 and H_2 sorption. For both gases, the pristine CNT and the bulk IL exhibited the largest and the smallest amount of sorption, respectively. These studies are important to understand H_2 and N_2 uptake in SILs, but relevant aspects such as the influence of pore size in a very strong confinement environment and its relation with the composition of the IL are yet to be addressed.

In an effort to shed some light on the capture and storage of nonpolar gases with small quadrupole moments in confined ILs, we have performed MC and MD simulations of H_2 and N_2 absorption in two different ILs confined in CNTs. The performance of the CNTs containing ILs was compared with that of the bulk ILs. Moreover, to analyze the role played by the IL, we examined a protic IL (PIL), ethylammonium nitrate (EAN), and an aprotic one (AIL), 1-ethyl-3-methylimidazolium tetrafluoroborate ([EMIM][BF_4]) (Fig. 1). Since the interactions in the ion pairs of PILs were reported to be stronger than those of AILs [49], it is of fundamental importance to understand the impact that these interactions can have on gas uptake. On the other hand, CNTs with radii

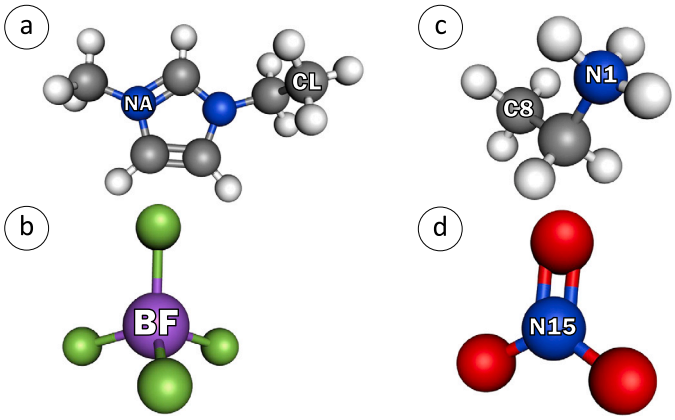

Fig. 1. Molecular structures of the ILs considered in this work: (a) 1-ethyl-3-methyl-imidazolium, (b) tetrafluoroborate, (c) ethylammonium and (d) nitrate. Grey, blue, white, green, violet and red correspond to carbon, nitrogen, hydrogen, fluorine, boron and oxygen.

Table 1
Correspondence between chiral indexes and CNT radii.

Chiral index							
(12,0)	(13,0)	(14,0)	(15,0)	(16,0)	(17,0)	(18,0)	(20,0)
Radius (Å)							
3.00	3.39	3.78	4.18	4.56	4.96	5.35	6.12

between 3.00 Å and 6.12 Å were chosen as a simple carbon-based pore model that can cope with the effect of the pore width variation on the structural features of the ILs and the resulting gas uptake. The largest nanotube employed in our work corresponds with the smallest one analyzed by Shi and Sorescu [48], which will allow us to analyze the performance of ILs in ultrahigh confinement for gas storage.

Thus, the aim of this work is to guide the design of promising adsorbents for gas storage analyzing the most suitable pore size for a given IL. For that purpose, first, we show the storage capacity for each of the considered ILs under confinement and in the bulk phase. Then, the structural and energetic characterization of the ILs confined in the carbon structure with different pore sizes was carried out to understand gas uptake from an atomistic point of view.

2. Simulation details

CNTs were generated using Visual Molecular Dynamics [50], and they were kept as rigid structures during the simulations since the influence of the framework flexibility on its adsorption properties was shown to be quite small [51]. Similarly, the helicity of the CNTs was observed to have little effect on the structure of other solvents confined inside [52], and on the adsorption of CO_2 [53]. Thus, we employed zigzag CNTs with chiral indexes ranging from 12 to 20, whose correspondence with the CNT internal radius (measured from the edge of the carbon atoms to the centre of the nanotube) is shown in Table 1.

Firstly, the CNTs were filled with the IL using the methodology of a nano-syringe described in detail in Ref. 54. Once the CNTs were filled with the IL, the number of ionic pairs inside the carbon structure ranged from 100 to 115 depending on the CNT considered, and their lengths ranged from 25 Å to 127 Å. Then, hybrid grand canonical Monte Carlo/molecular dynamics (GCMC/MD) simulations were carried out to evaluate the storage capacity of the ILs under confinement.

The OPLS-AA force field [55] was used to simulate the ILs, the CNT and their interaction with the absorbed gas molecules. The carbon atoms of the CNTs were represented using the atom `opls_147`. The parameterization of [EMIM][BF_4] was already used in Ref. 54, whereas the one used for EAN was reported in Ref. 56. Concerning the

gas molecules, 3-sites models were chosen in order to take into account their quadrupole moment. Nitrogen was modelled as two charged real atoms that have masses of 14.0067 u, charges of $-0.482e$ and Lennard-Jones parameters of $\sigma = 3.31 \cdot 10^{-1}$ nm and $\varepsilon = 2.99156 \cdot 10^{-1}$ kJ/mol. To maintain charge neutrality, a point charge of $+0.964e$ was placed at the centre of mass of the molecule [57]. On the other hand, hydrogen was parameterized as two charged real atoms that have masses of 1.008 u and charges of $+0.4932e$, constrained by a rigid bond and a charged virtual Lennard-Jones site whose parameters are $q = -0.9864e$, $\sigma = 2.958 \cdot 10^{-1}$ nm and $\varepsilon = 3.051336 \cdot 10^{-1}$ kJ/mol [58].

2.1. Hybrid grand canonical Monte Carlo/molecular dynamics simulations

Hybrid GCMC/MD simulations of H_2 and N_2 uptake were carried out using the LAMMPS package [59] in order to test the loading capacity of the confined ILs. These simulations were performed in the μVT ensemble at a temperature of 300 K, which was controlled by means of the Nosé-Hoover thermostat [60] with a relaxation time of 10 fs. All the bonds involving hydrogen atoms were kept constrained using the SHAKE algorithm [61]. The gas reservoir pressure, which is related to the chemical potential of the absorbate, was fixed to 100 bar. The MD simulations were carried out for 500 ps with a time step of 1 fs. The trial moves in the GCMC procedure were insertions and deletions (with equal probability), and they were attempted an average of 100 times every 10 fs. The centre of mass of the gas molecule is placed at an arbitrary insertion point inside the CNT and its orientation is chosen at random by rotating around this point. The same procedure was followed with bulk ILs for the purpose of comparison, the only difference being that these bulk simulations were performed in the μpT ensemble (at 300 K and 100 bar, as to ensure an equilibrium with the reservoir).

Then, a frame with the same gas occupancy as the average was selected as the input configuration for conventional MD simulations for each confined IL. Those CNTs in which the average gas uptake was lower than 5 gas molecules were replicated 2-3 times in order to improve the statistics in the MD simulations.

2.2. Molecular dynamics simulations

Once the storage capacity of the ILs confined in each of the CNTs was determined, MD simulations were performed in the NVT ensemble using the GROMACS 2020.6 software [62–64]. Firstly, all systems were relaxed using a conjugate gradients algorithm. The maximum step size and the tolerance were set to 0.01 nm and 0.1 kJ/(nm · mol), respectively. Second, a stabilization run was done at 300 K for 5 ns. Next, a production run for data collection was done for 20 ns at the same temperature, and the trajectory was recorded with a time interval of 1 ps. Finally, a run of 500 ps in which the velocities were saved at each step was carried out for the calculations of the Velocity Autocorrelation Functions (VACFs). The V-rescale thermostat introduced by Bussi et al. [65] was employed to control the temperature with a damping constant of 0.1 ps. Periodic boundary conditions were employed in the three directions, using a box large enough as to ensure that different replicas of the CNTs do not interact between them. All bonds containing hydrogen atoms were limited by the LINCS algorithm [66,67], with a fourth-order expansion of the constraint coupling matrix. For all the simulations, the equations of motion were integrated using a time step of 1 fs. The Verlet cutoff scheme with a buffer tolerance of 0.005 kJ/mol ps was used for long-range interactions in real space, whereas the Particle Mesh Ewald (PME) [68] method with a grid spacing of 0.12 nm and cubic interpolation was used to deal with long-range electrostatic interactions.

3. Results

3.1. Gas uptake

Firstly, we employed hybrid GCMC/MD calculations to study the N_2 and H_2 capture ability of ILs confined in carbon-based structures, with the aim of testing if a strong confinement regime is a suitable strategy for gas storage. The storage capacity obtained in the present GCMC/MD simulations is defined as the average number of gas molecules absorbed (once the ratio of insertion/deletion trials is stabilized) per IL pair inside each CNT, and it is plotted for both ILs in Fig. 2 as a function of the internal radius and chiral index of the CNT except for the EAN+ H_2 system, since for all CNTs no gas molecules were found to be absorbed after the Monte Carlo insertions. Gas storage capabilities of both ILs in bulk phase are included for comparison. It can be observed that in all cases the stored amount of gas under confinement tends to that in the bulk IL as the CNT diameter increases. Similarly, Shi and Luebke [47] reported a decreasing CO_2 and H_2 solubility in an IL confined in a silica slit pore when decreasing the degree of confinement. However, they did not analyze the impact of pore width variation on N_2 absorption. On the other hand, Shi and Sorescu [48] observed that the amount of H_2 absorbed in an IL confined in a CNT(20,20), which has a radius of 13.56 Å, was about 1.1-1.4 times larger than that in the bulk IL at moderate temperatures. In our case, gas storage capacity reaches a maximum at the narrow radius of 3.78 Å and 3.39 Å for [EMIM][BF_4] and EAN, respectively. Gas capture is observed to increase from nearly 0.4% up to 8%-25% when going from no confinement to those small pore sizes, thus demonstrating that confined ILs are more beneficial for capturing gases than bulk ILs. For both ILs, a second absorption peak is obtained for bigger CNTs, in particular, for those with internal radius of 4.56 Å and 4.96 Å for [EMIM][BF_4] and EAN, respectively. On the other hand, N_2 absorption ability is generally larger than that of H_2, probably due to the interaction between the highly polar ILs and the larger quadrupole moment of nitrogen molecules. In addition, confined [EMIM][BF_4] shows to be more efficient for gas uptake than EAN.

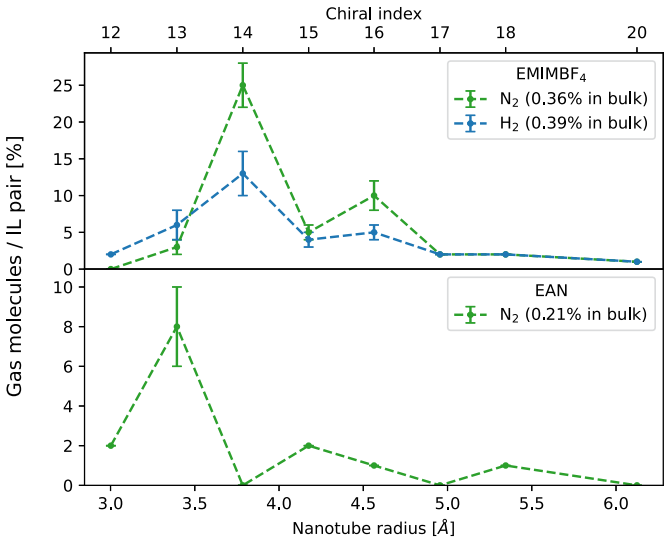

Fig. 2. N_2 (green) and H_2 (blue) uptake capacity with confined [EMIM][BF_4] (top) and EAN (bottom) as a function of the CNTs internal radius and their chiral index. Gas storage capabilities of both ILs in bulk phase are included for the purpose of comparison. Error bars represent the standard deviation of the average number of gas molecules adsorbed.

The different storage capacities can be analyzed in terms of the empty space available within the CNTs to dissolve the gas molecules. This free volume is strongly dependent on the interplay between ionic interactions and pore size, as they govern the structural conformation of the IL inside the CNTs. Thus, we have calculated the percentage of accessible free volume by inserting trial molecules in randomly selected positions and orientations within the CNTs. The trial molecules consist of two hard spheres separated by a rigid bond, mimicking the structure of the gas molecules inserted in the μVT simulations. Thus, the inserted spheres have radii of 1.2 and 1.55 Å for H_2 and N_2, respectively [69], whereas the separation between them was set to 0.7414 and 1.0977

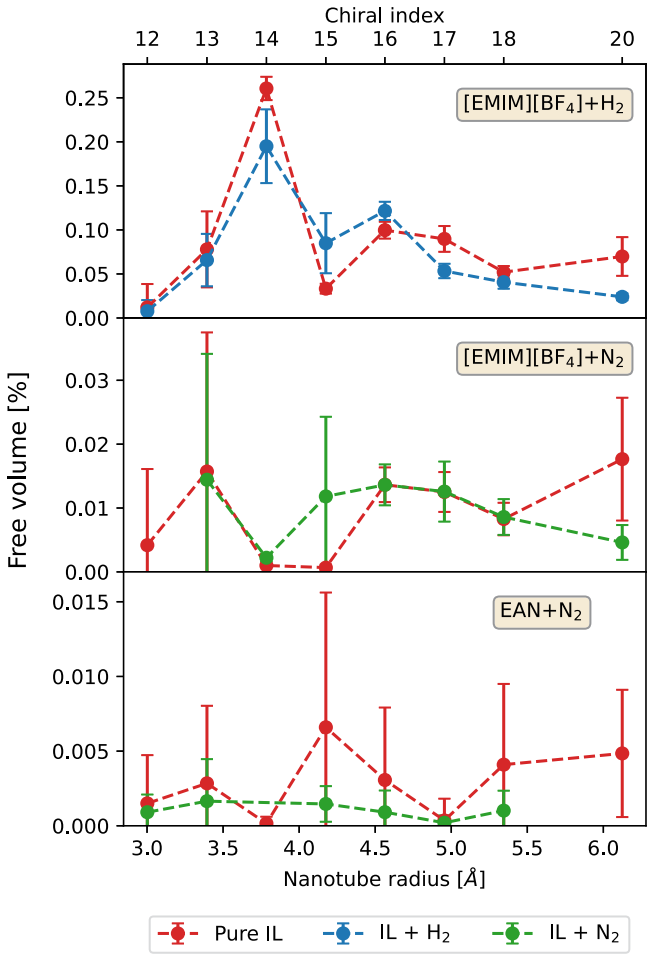

Fig. 3. Percentage of accessible free volume for H_2 in [EMIM][BF_4] (top), N_2 in [EMIM][BF_4] (centre) and H_2 in EAN (bottom). The colours indicate the systems in which the insertions were performed. Error bars represent the standard deviation of the accessible free volume.

Å, following the MD parameters for molecular hydrogen and nitrogen, respectively. The estimation was done for pure IL confined inside the CNTs, and also for the IL loaded with gas but without taking into account the volume occupied by the gas molecules. The percentage of free volume was defined as the ratio between the number of accepted insertions and the number of trials, and it was computed trying $5 \cdot 10^6$ times per frame. The results are included in Fig. 3 as a function of CNT internal radius and the corresponding chiral index. It can be seen that those CNTs for which we observed the maximum gas capture only correspond with those with the maximum amount of free volume for the system where H_2 is absorbed. For N_2, there is no apparent relation between available free volume and gas capture. This is quite unexpected, since the extra free volume in the restricted space of the CNTs due to some frustrated arrangement of the ions compared to bulk IL has been identified as the basis of the remarkable enhancement of gas uptake [21]. However, our results indicate that the absorption of nitrogen molecules is not only governed by the amount of empty accessible space within the system, but also by the interactions between the different species, unlike H_2 molecules. Hydrogen is a molecule with a very small size and low intermolecular interactions, due to which it always behaves nearly as an ideal gas. In fact, only dipole-quadrupole interactions, which are slightly stronger for nitrogen molecules, are significant in these systems.

In order to gain greater molecular understanding of the nanoconfinement effect on the gas absorption mechanism, the observed storage capacities were evaluated both from the structural and the energetic point of view. As it is well-known, the confinement of ILs in nanoscale geometries leads to a different physical and chemical behaviour, such as changes in the wetting behaviour or the freezing-melting temperature [70]. Also, the way ILs reorganize when encapsulated inside CNTs was previously reported by Montes-Campos and coworkers [54], showing that it is restricted by the carbon surface. Consequently, their study showed that, when the CNT width reaches the characteristic ion pair size, the structural conformation of the ions changes from a highly ordered one dimensional array to a more disordered structure in which the ions are arranged forming rings in the radial direction.

Thus, in the present work the effect of CNT channel size was investigated by calculating the number of IL layers formed inside each of the CNTs. The number of layers is calculated by randomly inserting planes perpendicular to the tubular axis in the simulation box. Then, for each molecule, the plane that intersects the highest number of molecules is selected (see Fig. S1 of the Supporting Information). The amount of ionic species cut through by this plane is the number of layers associated to that molecule, and the global number of layers is obtained as an average over all molecules and frames of the simulation. Planes that intersect no molecules are disregarded. The number of layers as a function of the CNTs internal radius and the corresponding chiral index are shown in Fig. 4, in which the colour gradient identifies the different number of layers within the CNTs.

Focusing on [EMIM][BF_4], it can be observed that, as the CNT diameter increases, the accommodation of the ions changes from one layer [in CNT(12,0), CNT(13,0) and CNT(14,0)] to two layers [in CNT(15,0) and CNT(16,0)], and then more complex structures are adopted. Interestingly, the two previously mentioned peaks of the gas uptake capacity obtained for CNT(14,0) and CNT(16,0) in Fig. 2 correspond to the transition from one to two layers, and from two to three layers, respectively. This indicates that the maximum gas capture for a given structure of layers takes place right before reaching a nanotube size that allows the formation of one more layer, which usually shows a lower absorption capacity. This can be clearly appreciated in those CNTs that let the formation of $1-2$ layers, but for bigger CNTs there are probably some other effects playing a role, since they allow the appearance of more complex conformations. The same behaviour is observed in the case of EAN, where the gas uptake maxima were found for CNT(13,0) and CNT(15,0), which in turn correspond to the largest nanotubes capable of hosting one and two layers, respectively. The fact that maximum gas uptake values are registered for those CNTs in which the IL possesses a greater degree of conformational freedom is further confirmed by the analysis of the distribution of ion orientations. This is included in Fig. S2 of the Supporting Information, and the most remarkable feature is that in those CNTs in which the number of layers is about to increase, that is, for the biggest CNT in each subplot, the ions are accommodated showing a wider variety of orientations.

As we previously hypothesized, the existence of cavities capable of encapsulating H_2 or N_2 molecules in terms of size seems insufficient to explain the gas uptake mechanism, specially in the case of N_2. This could be due to relevant interactions between gas molecules and the IL or the CNT, which could result in cavities where hosting a gas molecule is not energetically favourable, even though it is big enough to accommodate it. To perform an evaluation of free volume that takes this effect into account, we calculated

$$\phi = \langle \min\left(1, e^{-\beta(E-\mu)}\right) \rangle, \tag{1}$$

where E is the energy of a gas molecule inserted in a random position inside a given CNT filled with pure IL, μ is the chemical potential of the reservoir (which was modelled as an ideal gas), $\beta = 1/k_B T$, and the brackets indicate averaging over many IL configurations and gas molecule insertions. This expression is equivalent to the fraction of accepted insertions during GCMC simulations in a nanotube without any gas molecules absorbed. Gas molecules were modelled using the same parameters as in the MD simulations, and both Coulomb and LJ contributions were taken into account for the calculation of E. A total of

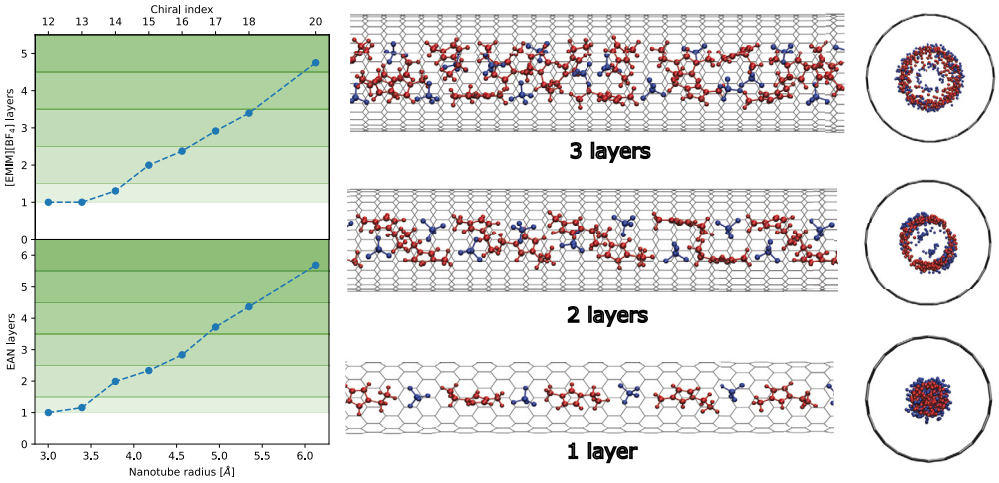

Fig. 4. Left: Number of ionic layers formed under confinement by [EMIM][BF_4] (top) and EAN (bottom) as a function of the CNTs internal radii and their chiral index. The colour gradient is meant as a guide to the eye, to indicate the increasing number of layers. Right: Snapshots taken from CNTs with chiral indices (from bottom to top) 12, 15 and 17 and filled with [EMIM][BF_4] depicting the arrangement of ions in various layers. Cations are coloured red, while anions are blue.

$2 \cdot 10^4$ configurations were extracted from production runs in intervals of 1 ps, and each one was sampled using $4 \cdot 10^4$ insertions.

The results are shown in Fig. 5. It can be seen that in general, a much more similar behaviour to the gas uptake profiles of Fig. 2 is recovered. In fact, for all studied systems, the first peak in ϕ corresponds to the CNT that exhibits the highest gas uptake, showing both that this average is indeed capable of predicting gas uptake maxima, and that gas absorption in the confined regime is highly dependent on the interactions between the host molecules and the rest of the system, unlike bulk systems where the relevant metric is just the probability of cavities capable of hosting gas molecules being formed inside the IL [56]. As for the secondary uptake peaks, it can be seen that they are correctly predicted in the case of H_2 in [EMIM][BF_4] and N_2 in EAN, whereas for N_2 in [EMIM][BF_4] the absorption peak is predicted for CNT(17,0), while the absorption peak is found in CNT(16,0). This could be due to the complex structuring of the IL giving raise to additional effects, which is plausible since CNT(16,0) and CNT(17,0) exhibit a two and three layer structure, respectively, as seen in Fig. 4. Finally, it is interesting to note that for the same gas (N_2), the values of ϕ are greater for [EMIM][BF_4] than for EAN, which is consistent with the fact that the former is capable of hosting more gas molecules than the latter.

In addition to the energetically accessible free volume, the interactions between the gas molecules and the IL ions, as well as those between the gas molecules and the CNTs were calculated using GROMACS tools. The corresponding results are plotted in Fig. 6 as a function of the CNTs internal radius and their chiral index. The total interaction energies are much stronger (more negative) for those CNTs in which we observed a great absorption ability [CNT(14,0) and CNT(16,0) for [EMIM][BF_4] and CNT(13,0) and CNT(15,0) for EAN] and they become weaker as the radius of the CNT increases. Also, the interaction energies for the cation and the anion are similar, the latter being slightly weaker for most cases. The results clearly indicate that gas interactions are mainly driven by the CNT contribution, which is stronger for N_2 than for H_2 in the presence of the same IL, and it is also stronger for N_2 absorbed in [EMIM][BF_4] than in EAN. These findings are consistent with the gas molecules being placed within the volume of the IL but close to the CNT wall, as it will be confirmed later with the analysis of the probability density distributions of the components of the mixture. In addition, gas-solid interactions are the most significant, which explains the fact that gas uptake in ILs increases in a nanoconfined environment compared to the bulk.

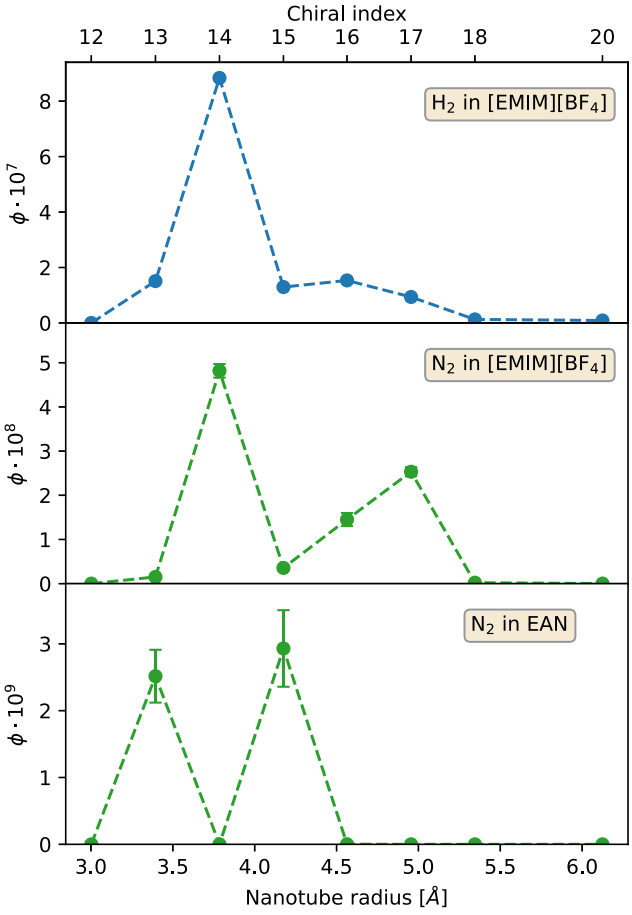

Fig. 5. Energetic accessible free volume for probe radii about the size of H_2 (top) and N_2 (centre) molecules in confined [EMIM][BF_4], and N_2 molecules in confined EAN (bottom) as a function of the CNTs chiral index.

3.2. Structure

IL structure confined in the CNTs is further quantified by analyzing the distribution of the IL ions in the radial direction of the CNTs before and after the gas capture. To take into account the possible formation of polar and apolar domains, the radial density profiles of the cations

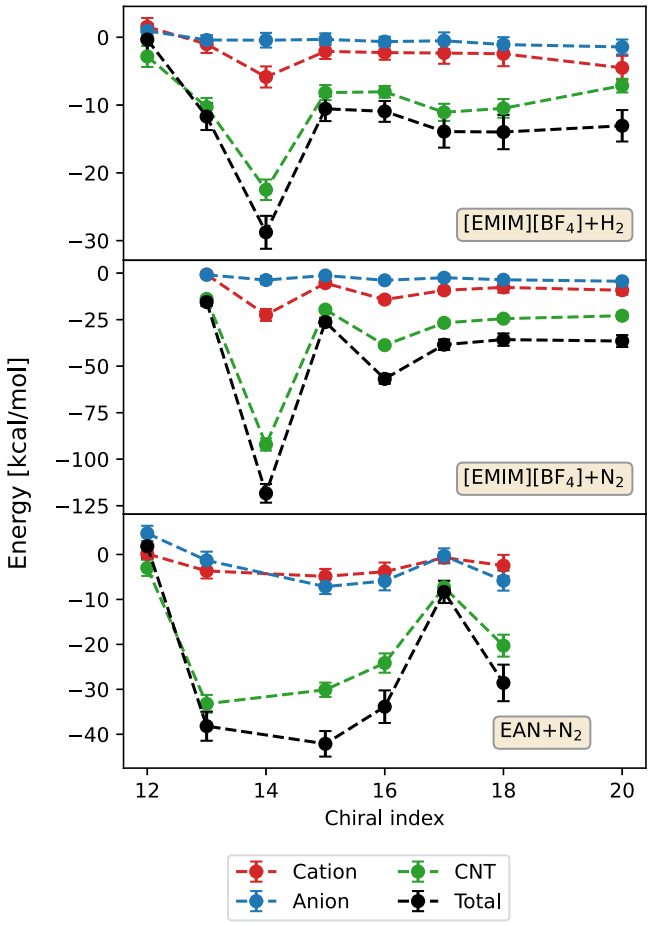

Fig. 6. Interaction energy between gas molecules and other components of the systems as a function of the CNTs chiral index for H_2 confined in [EMIM][BF_4] (top), N_2 confined in [EMIM][BF_4] (centre) and N_2 confined in EAN (bottom).

were calculated both for the polar head and the alkyl tail. Thus, for $[EMIM]^+$ the chosen atoms were the nitrogen atom NA and the carbon atom CL of Fig. 1 while for $[BF_4]^-$ the boron atom BF was used. On the other hand, the atoms taken into account to analyze the PIL were the nitrogen atom N1 and the carbon atom C8 for $[EA]^+$, and the nitrogen atom N15 for $[NO_3]^-$. The number density profiles corresponding to the CNTs where gas uptake is maximized, along with the ones with the greater chiral indices, are shown in Fig. 7 (the results for all the studied systems are shown in Fig. S3 of the Supporting Information). Overall, the presence of sharp peaks indicates a strong modification of the structure of the liquid when it interacts with the CNT. Moreover, as the radii of the CNTs are increased, new peaks appear, signalling the existence of extra IL layers in addition to the one closest to the interface, as already reported by Pensado *et al.* in Ref. [71].

For the CNTs corresponding to gas uptake maxima (top row of Fig. 7), it can be seen that, while N_2 absorption does not result in changes to the density profiles, this is not the case for H_2, which forces [EMIM][BF_4] molecules to slightly modify their structure to accommodate it. This could in part explain the fact that H_2 is not absorbed in EAN filled CNTs, since this IL is more tightly packed than [EMIM][BF_4], and thus it would be more difficult for it to change its structure, even if this change is small. On the other hand, for bigger CNTs (bottom row of Fig. 7) this effect disappears, and neither H_2 nor N_2 cause a rearrangement of the IL. This is consistent with the fact that in the bulk regime H_2 molecules tend to accommodate into the interstitial voids of the IL network without significantly disrupting its structure [56].

To obtain a deeper understanding of the gas storage mechanism, it is also relevant to know in which regions the absorption of gas molecules takes place. That is, whether gas molecules are absorbed within the volume of the IL—as observed by Harmanly et al. in a carbon-based material—or they are instead absorbed close to the pore walls [21]. This last situation was reported by Shi and Luebke for silica slit pores [47]. In order to enlighten this point, we determined the radial probability density distribution of both ILs and the gas molecules, which are shown in Fig. 8 for the CNTs with the greatest gas absorption (top row) and the ones with the largest radii (bottom row). All of them can be found in Fig. S4 of the Supporting Information. For both IL systems, the absorption of gas molecules within the region populated by the atoms of the IL is clearly appreciated regardless of the size of the CNT. This fact further supports the initial hypothesis of this work: energetically favourable free volume spots for gas molecules appear under a strong confinement of the IL. However, the energetic contribution of the CNT to the gas molecules favours them positioning closer to the wall in most cases. As an exception to this, there is a peak of H_2 molecules near the axis in the CNT(20,0) filled with [EMIM][BF_4]. Notably, this is related to the change in energy contributions in Fig. 6, with that peak being responsible for the more favourable energy contribution by the cation. Regarding the N_2 distributions, there is also some uptake near the axis in that same CNT. Contrarily, the CNT(18,0) filled with EAN does not reflect any absorption in that region due to the high packing density of this IL, as mentioned above.

To further confirm that, despite being weakly interacting gases, nitrogen and hydrogen uptake and their accommodation inside the nanotubes is not only governed by molecular packing effects, the previous results can be compared with a toy model of the IL+CNT+gas system in which both ions and gas molecules are replaced by chargeless hard spheres. More details on these calculations can be read in the Supporting Information. The gas uptake profile is depicted in Fig. 9. The results show a striking difference between the toy model and the simulations. The gas uptake profile for the model shows a single maximum, in contrast with the multiple ones observed for N_2 systems. Moreover, the value of the maximum is very close to the bulk absorption value, to which large CNTs converge, in contrast with the simulated ones, where gas uptake is significantly higher in some CNTs than for the bulk regime. This shows to a certain degree that gas uptake is not determined solely by the packing of the IL molecules, as evidenced by its lack of correlation with free volume. This conclusion is further supported by the probability distributions obtained for the toy model, which are included in Fig. S5 of the Supporting Information and can be compared with the ones obtained from simulations (Fig. S4). It can be seen that in the toy model, gas particles have a tendency to leave the IL-rich regions and accommodate into in the empty region between the IL and the CNT. Moreover, the gas population within the IL is low, and only becomes noticeable for large CNTs. This is not observed in the simulations, where gas molecules are hosted within the liquid, and are never observed alone in the surface of the CNT. The first effect can be attributed to the fact that molecules in the toy model are structureless, and therefore expected to leave less interstitial voids, leading to the lower presence of gas within the IL. However, the abundance of gas in the regions where no IL molecules are present is not clearly correlated with the details of the structural picture. This suggests that interactions beyond simple hard-core repulsion, such as electrostatic energies, must play an important role in the absorption process of these gases, as previously discussed.

Finally, the analysis of the single-particle dynamics was accomplished through the calculation of the centre-of-mass VACFs of the gas molecules. The normalized VACF is computed as

$$C(t) = \frac{\langle \vec{v}(t) \cdot \vec{v}(0) \rangle}{\langle \vec{v}(0) \cdot \vec{v}(0) \rangle}, \tag{2}$$

where $\vec{v}(t)$ is the velocity of the centre-of-mass of the molecule at time t and the brackets indicate the ensemble average. The results are included in Fig. S6 of the Supporting Information. From these autocorrelation

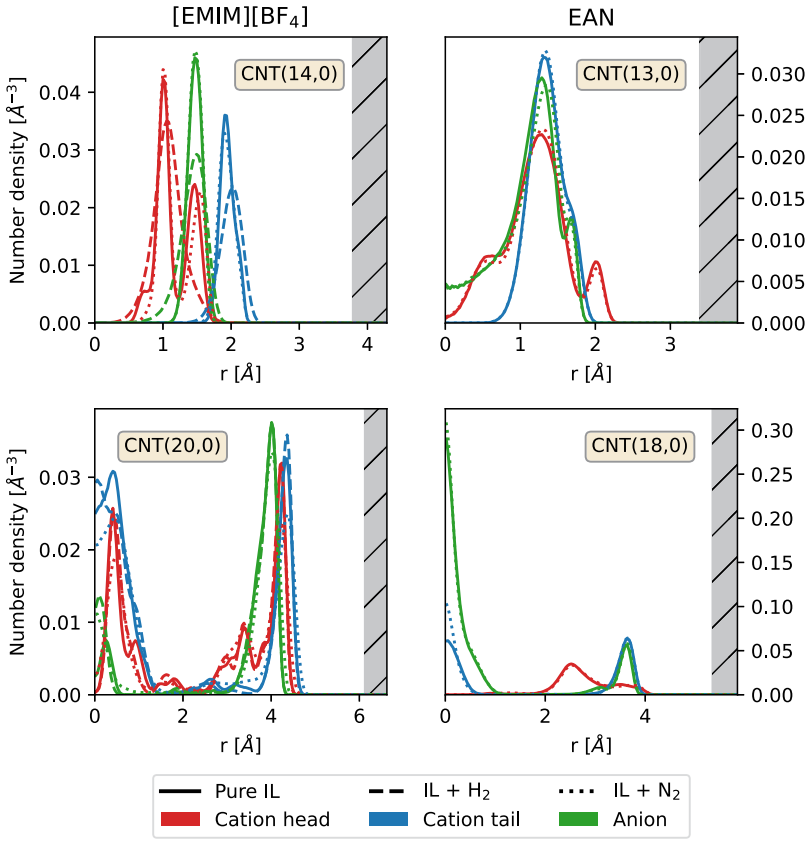

Fig. 7. Number density profiles in the CNT radial direction. Solid, dashed and dotted lines correspond with the distribution of the ions before gas absorption, after the absorption of H_2, and after the absorption of N_2, respectively.

functions the vibrational Density of States (vDOS) can be obtained in a straightforward way as the Fourier transform of the VACFs

$$I(\omega) = \left| \int_0^\infty e^{-i\omega t} C(t) dt \right|^2 \tag{3}$$

We consider here that $I(\omega)$ is normalized such that

$$\int_0^\infty I(\omega) d\omega = 1 \tag{4}$$

The results obtained for all gas molecules absorbed in the different CNTs are plotted in Fig. 10. There we can observe that the profiles are clearly blue-shifted as the size of the CNTs increases, which is consistent with the gas molecules being more tightly packed in regions in which the free volume is less energetically favourable, as it was shown in Fig. 5. Therefore, those vDOS at low frequencies can be attributed to IL configurations with looser packing where gas molecules are stored and have larger mean free paths. As CNT radius increases, the liquid inside becomes more bulk-like, leading to a tighter packing, and hence, to the blue shift present in the spectra. This is consistent with the vDOS of N_2 molecules absorbed in EAN being the least displaced, since the packing of this IL leaves the least free volume, and thus exhibits smaller cavities.

4. Conclusions

In this work, the gas uptake mechanism of H_2 and N_2 in zigzag CNTs with varying chiral index was studied by means of classical molecular dynamic simulations and hybrid grand canonical Monte Carlo/molecular dynamics simulations at $T = 300$ K. CNTs are filled with one aprotic IL ([EMIM][BF_4]) and one protic IL (EAN).

Firstly, the gas molar fraction absorbed in each case was determined by the grand canonical Monte Carlo/molecular dynamics simulations by inserting gas molecules into IL confined in CNTs. These simulations revealed that gas storage capacity reaches a maximum for CNTs with radii of 3.78 Å and 3.39 Å filled with [EMIM][BF_4] and EAN, respectively. An increase in the absorption of gas molecules up to 25% was found for these CNTs, which is much greater than the 0.4% observed in bulk IL. Secondary absorption peaks were also observed for both ILs in those CNTs with internal radii of 4.56 Å and 4.96 Å for [EMIM][BF_4] and EAN, respectively. In addition, N_2 absorption ability appears to be larger than that of H_2, and [EMIM][BF_4] shows to be more efficient for gas storage than EAN regardless of the channel size of the confining CNTs. Finally, no H_2 molecules were found to be absorbed in EAN filled CNTs, which is in agreement with the low free volume in the liquid.

To understand the mechanism of gas capture, accessible free volume was analyzed as it is a key factor in gas absorption by ILs. These results show that the solvation energetics must also be taken into account for a correct understanding of N_2 uptake in confined ionic solvents. This is in contrast with the case of H_2 absorption, which can be properly explained solely by free volume calculations. Moreover, the greatest gas storage capacity was shown to be correlated with structural changes in the ILs, namely the number of ionic layers within the CNTs, which in turn affect the available volume for gas absorption.

Finally, the structural analysis reveals the preference of both gas molecules to be placed in the IL-rich region as energy-favoured structural voids appear due to the confinement of the ILs. Also the more relevant energetic contribution to the gas molecules is the one of the CNT, favouring these molecules to accommodate themselves closer to the carbon wall. On the other hand, the study of the single particle dynamics shows that the vDOS is blue-shifted with increasing radii of the CNTs, which is attributed to the gas molecules being more densely packed in areas where the free volume is less energetically favourable.

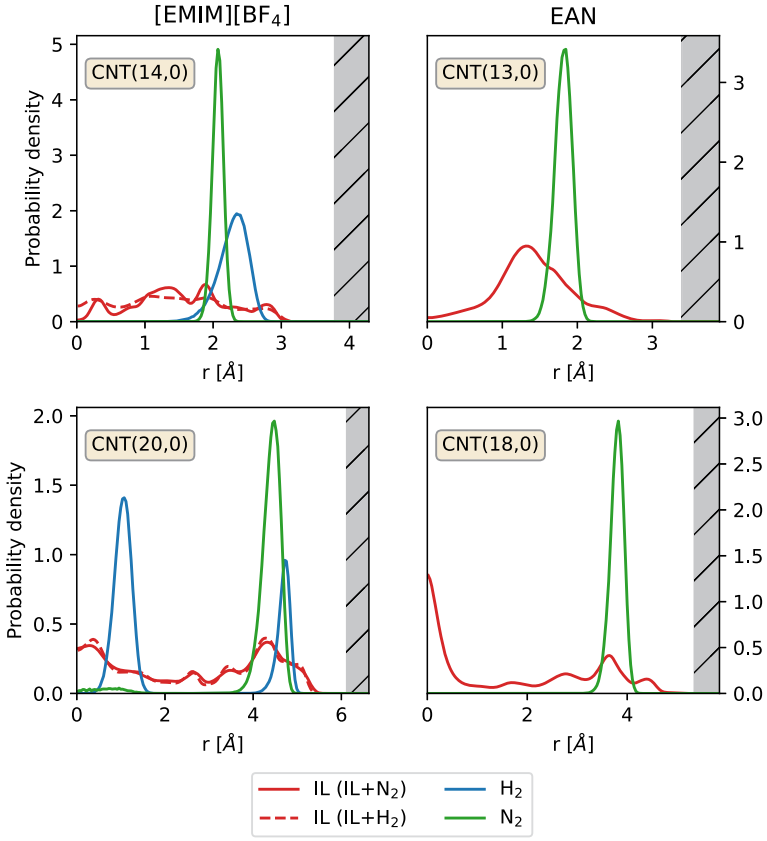

Fig. 8. Probability density distribution of finding an atom belonging to the IL (red), H_2 gas (blue) or N_2 gas (green) at a certain distance from the radial axis of the CNT. For each IL, the CNT with the greatest gas absorption (top row) and the one with the largest radius (bottom row) are depicted. For the IL, solid lines correspond to IL+ N_2 systems, while dashed lines represent IL+ H_2.

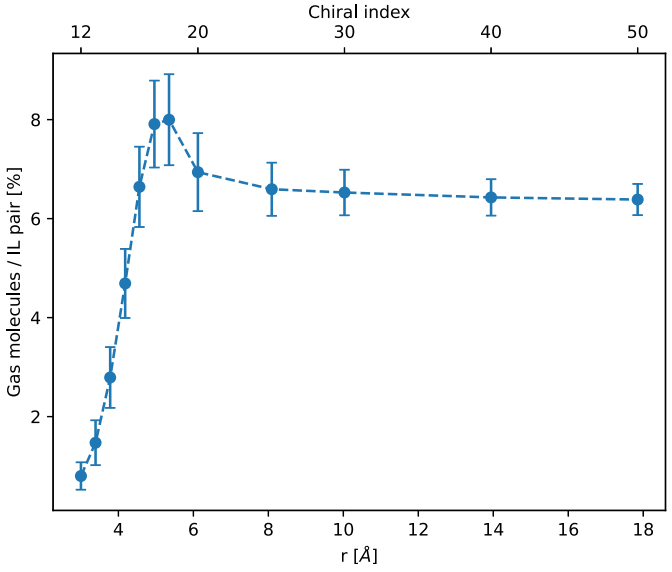

Fig. 9. Gas uptake in the hard sphere model as a function of CNT radius and chiral index. Errorbars show the standard deviation.

In conclusion, this work confirms that a strong confinement of ILs inside a porous host can greatly increase their gas storage capacity, allowing for the accommodation of larger amounts of gas within energetically favourable structural voids that emerge as a result of modifications in the structural conformation of the ILs. The influence of pore shape and geometry in gas capture and storage in more complex porous materials will be examined in a future work.

CRediT authorship contribution statement

Martín Otero-Lema: Writing – review & editing, Writing – original draft, Visualization, Validation, Software, Methodology, Investigation, Formal analysis. **Raúl Lois-Cuns:** Writing – review & editing, Writing – original draft, Visualization, Validation, Software, Methodology, Investigation, Formal analysis. **Pablo Martínez-Crespo:** Writing – review & editing, Writing – original draft, Visualization, Validation, Software, Methodology, Investigation, Formal analysis. **Alejandro Rivera-Pousa:** Writing – review & editing, Writing – original draft, Visualization, Validation, Software, Methodology, Investigation, Formal analysis. **Hadrián Montes-Campos:** Writing – review & editing, Writing – original draft, Visualization, Validation, Supervision, Software, Project administration, Methodology, Investigation, Formal analysis, Conceptualization. **Trinidad Méndez-Morales:** Writing – review & editing, Writing – original draft, Visualization, Validation, Supervision, Software, Project administration, Methodology, Investigation, Funding acquisition, Formal analysis, Conceptualization. **Luis M. Varela:** Writing – review & editing, Visualization, Supervision, Project administration, Funding acquisition, Formal analysis, Conceptualization.

Declaration of competing interest

The authors declare that they have no known competing financial interests or personal relationships that could have appeared to influence the work reported in this paper.

Data availability

Input files and analysis scripts are available at https://doi.org/10.5281/zenodo.10495511.

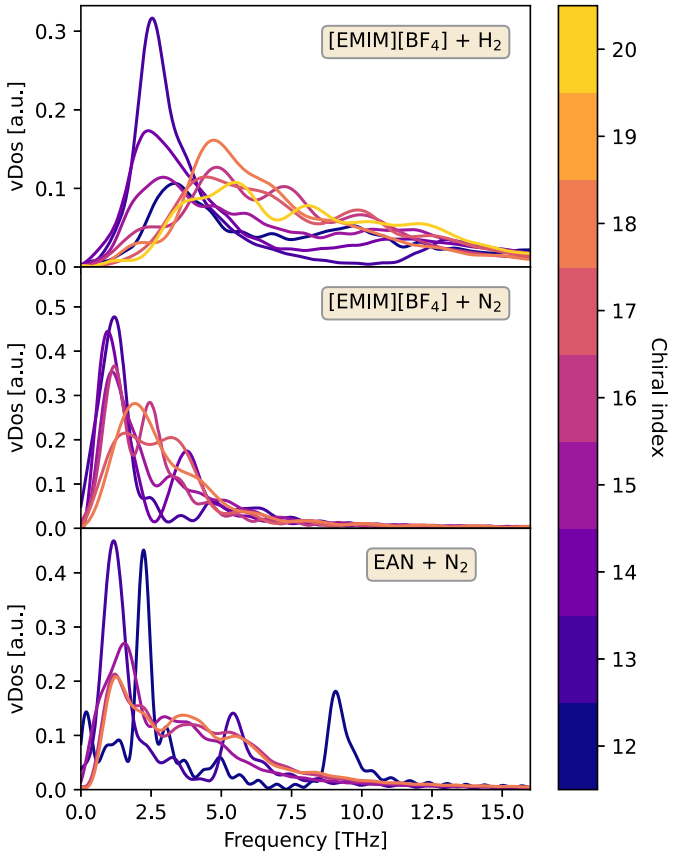

Fig. 10. Vibrational density of states of (top) H_2 molecules absorbed in [EMIM][BF_4], (centre) N_2 molecules absorbed in [EMIM][BF_4] and, (bottom) N_2 molecules absorbed in EAN.

Acknowledgement

The financial support of the Spanish Ministry of Science and Innovation (PID2021-126148NA-I00 funded by MCIN/AEI/10.13039/501100011033/FEDER, UE) is gratefully acknowledged. Moreover, this work was funded by the Xunta de Galicia (GRC ED431C 2020/10). A. R. P. thanks the Spanish Ministry of Education for his FPU18/01597 grant. M. O. L. and P. M. C. wish to thank the Xunta de Galicia for their "Axudas de apoio á etapa predoutoral" grant (ED481A 2022/236 and ED481A 2022/045). T. M. M. acknowledges her contract funded by the pilot program of the USC for the recruitment of Distinguished research personnel—call 2021 under the agreement between the USC and the Santander Bank for 2021–2024. This publication and the contract of T. M. M. are part of the grant RYC2022-036679-I, funded by MCIN/AEI/10.13039/501100011033 and FSE+. H. M. C. thanks the USC for his "Convocatoria de Recualificación do Sistema Universitario Español-Margarita Salas" postdoctoral grant under the "Plan de Recuperación Transformación" program funded by the Spanish Ministry of Universities with European Union's NextGenerationEU funds. R. L. C. acknowledges his Predoctoral Contract under the framework of the project PID2021-126148NA-I00 funded by MCIN/AEI/10.13039/501100011033/FEDER, UE. This work was supported by the Fundacão para a Ciência e Tecnologia (FCT) (funded by national funds through the FCT/MCTES (PIDDAC)) to CIQUP, Faculty of Science, University of Porto (Project UIDB/00081/2020), IMS-Institute of Molecular Sciences (LA/P/0056/2020).

Appendix A. Supplementary material

Supplementary material related to this article can be found online at https://doi.org/10.1016/j.molliq.2024.124909.

References

[1] H.C. Lau, S. Ramakrishna, K. Zhang, A.V. Radhamani, The role of carbon capture and storage in the energy transition, Energy Fuels 35 (2021) 7364–7386.
[2] A.M. Oliveira, R.R. Beswick, Y. Yan, A green hydrogen economy for a renewable energy society, Curr. Opin. Chem. Eng. 33 (2021) 100701.
[3] G. Chehade, I. Dincer, Progress in green ammonia production as potential carbon-free fuel, Fuel 299 (2021) 120845.
[4] S. Kumar, R. Srivastava, J. Koh, Utilization of zeolites as co2 capturing agents: advances and future perspectives, J. CO2 Util. 41 (2020) 101251.
[5] R.V. Siriwardane, M.-S. Shen, E.P. Fisher, Adsorption of co2, n2, and o2 on natural zeolites, Energy Fuels 17 (2003) 571–576.
[6] M. Mohan, V.K. Sharma, E.A. Kumar, V. Gayathri, Hydrogen storage in carbon materials—a review, Energy Storage 1 (2019) e35.
[7] J.W. Yoon, H. Chang, S.-J. Lee, Y.K. Hwang, D.-Y. Hong, S.-K. Lee, J.S. Lee, S. Jang, T.-U. Yoon, K. Kwac, et al., Selective nitrogen capture by porous hybrid materials containing accessible transition metal ion sites, Nat. Mater. 16 (2017) 526–531.
[8] J. Yu, L.-H. Xie, J.-R. Li, Y. Ma, J.M. Seminario, P.B. Balbuena, Co2 capture and separations using mofs: computational and experimental studies, Chem. Rev. 117 (2017) 9674–9754.
[9] S.S. Han, H. Furukawa, O.M. Yaghi, W.A. Goddard III, Covalent organic frameworks as exceptional hydrogen storage materials, J. Am. Chem. Soc. 130 (2008) 11580–11581.
[10] J.L. Anderson, J.K. Dixon, J.F. Brennecke, Solubility of co2, ch4, c2h6, c2h4, o2, and n2 in 1-hexyl-3-methylpyridinium bis (trifluoromethylsulfonyl) imide: comparison to other ionic liquids, Acc. Chem. Res. 40 (2007) 1208–1216.
[11] Z. Lei, C. Dai, B. Chen, Gas solubility in ionic liquids, Chem. Rev. 114 (2014) 1289–1326.
[12] J. Huang, A. Riisager, R.W. Berg, R. Fehrmann, Tuning ionic liquids for high gas solubility and reversible gas sorption, J. Mol. Catal. A, Chem. 279 (2008) 170–176.
[13] W.F. Elmobarak, F. Almomani, M. Tawalbeh, A. Al-Othman, R. Martis, K. Rasool, Current status of co2 capture with ionic liquids: development and progress, Fuel 344 (2023) 128102.
[14] R. Santiago, J. Lemus, A.X. Outomuro, J. Bedia, J. Palomar, Assessment of ionic liquids as h2s physical absorbents by thermodynamic and kinetic analysis based on process simulation, Sep. Purif. Technol. 233 (2020) 116050.
[15] T. Welton, Ionic liquids: a brief history, Biophys. Rev. 10 (2018) 691–706.
[16] K.N. Marsh, J.A. Boxall, R. Lichtenthaler, Room temperature ionic liquids and their mixtures—a review, Fluid Phase Equilib. 219 (2004) 93–98.
[17] S.P. Ventura, A.M. Gonçalves, T. Sintra, J.L. Pereira, F. Gonçalves, J.A. Coutinho, Designing ionic liquids: the chemical structure role in the toxicity, Ecotoxicology 22 (2013) 1–12.
[18] N.V. Plechkova, K.R. Seddon, Ionic Liquids: "Designer" Solvents for Green Chemistry, Wiley Online Library, 2007.
[19] K. Ghandi, A review of ionic liquids, their limits and applications, Green Sustain. Chem. 2014 (2014).
[20] T. Selvam, A. Machoke, W. Schwieger, Supported ionic liquids on non-porous and porous inorganic materials—a topical review, Appl. Catal. A, Gen. 445 (2012) 92–101.
[21] I. Harmanli, N.V. Tarakina, M. Antonietti, M. Oschatz, "Giant" nitrogen uptake in ionic liquids confined in carbon pores, J. Am. Chem. Soc. 143 (2021) 9377–9384.
[22] J.J. Close, K. Farmer, S.S. Moganty, R.E. Baltus, Co2/n2 separations using nanoporous alumina-supported ionic liquid membranes: effect of the support on separation performance, J. Membr. Sci. 390 (2012) 201–210.
[23] J. Wang, H. Ding, B.-c. Cao, X. Huang, Effect of ionic liquid confinement on co2 solubility and permeability characteristics, Greenh. Gases 7 (2017) 474–485.
[24] D. Chen, W. Ying, Y. Guo, Y. Ying, X. Peng, Enhanced gas separation through nanoconfined ionic liquid in laminated mos2 membrane, ACS Appl. Mater. Interfaces 9 (2017) 44251–44257.
[25] F. Rahmani, P. Scovazzo, M.A. Pasquinelli, S. Nouranian, Effects of ionic liquid nanoconfinement on the co2/ch4 separation in poly (vinylidene fluoride)/1-ethyl-3-methylimidazolium thiocyanate membranes, ACS Appl. Mater. Interfaces 13 (2021) 44460–44469.
[26] A. Labropoulos, G.E. Romanos, E. Kouvelos, P. Falaras, V. Likodimos, M. Francisco, M. Kroon, B. Iliev, G. Adamova, T.J. Schubert, Alkyl-methylimidazolium tricyanomethanide ionic liquids under extreme confinement onto nanoporous ceramic membranes, J. Phys. Chem. C 117 (2013) 10114–10127.
[27] M. Zhang, A. Yu, X. Wu, P. Shao, X. Huang, D. Ma, X. Han, J. Xie, X. Feng, B. Wang, Sealing functional ionic liquids in conjugated microporous polymer membrane by solvent-assisted micropore tightening, Nano Res. (2021) 1–6.
[28] J.M. Vicent-Luna, J.J. Gutiérrez-Sevillano, J.A. Anta, S. Calero, Effect of room-temperature ionic liquids on co2 separation by a cu-btc metal–organic framework, J. Phys. Chem. C 117 (2013) 20762–20768.
[29] M. Mohamedali, A. Henni, H. Ibrahim, Markedly improved co2 uptake using imidazolium-based ionic liquids confined into hkust-1 frameworks, Microporous Mesoporous Mater. 284 (2019) 98–110.
[30] Y. Chen, Z. Hu, K.M. Gupta, J. Jiang, Ionic liquid/metal–organic framework composite for co2 capture: a computational investigation, J. Phys. Chem. C 115 (2011) 21736–21742.

[31] K.M. Gupta, Y. Chen, J. Jiang, Ionic liquid membranes supported by hydrophobic and hydrophilic metal–organic frameworks for co2 capture, J. Phys. Chem. C 117 (2013) 5792–5799.
[32] K.M. Gupta, Y. Chen, Z. Hu, J. Jiang, Metal–organic framework supported ionic liquid membranes for co 2 capture: anion effects, Phys. Chem. Chem. Phys. 14 (2012) 5785–5794.
[33] Z. Tian, S. Dai, D.-e. Jiang, Confined ionic liquid in an ionic porous aromatic framework for gas separation, ACS Appl. Polym. Mater. 1 (2018) 95–102.
[34] Z. Li, Y. Xiao, W. Xue, Q. Yang, C. Zhong, Ionic liquid/metal–organic framework composites for h2s removal from natural gas: a computational exploration, J. Phys. Chem. C 119 (2015) 3674–3683.
[35] W. Xue, Z. Li, H. Huang, Q. Yang, D. Liu, Q. Xu, C. Zhong, Effects of ionic liquid dispersion in metal-organic frameworks and covalent organic frameworks on co2 capture: a computational study, Chem. Eng. Sci. 140 (2016) 1–9.
[36] M. Mohamedali, H. Ibrahim, A. Henni, Incorporation of acetate-based ionic liquids into a zeolitic imidazolate framework (zif-8) as efficient sorbents for carbon dioxide capture, Chem. Eng. J. 334 (2018) 817–828.
[37] I. Yasmeen, A. Ilyas, Z. Shamair, M.A. Gilani, S. Rafiq, M.R. Bilad, A.L. Khan, Synergistic effects of highly selective ionic liquid confined in nanocages: exploiting the three component mixed matrix membranes for co2 capture, Chem. Eng. Res. Des. 155 (2020) 123–132.
[38] O. Tzialla, C. Veziri, X. Papatryfon, K. Beltsios, A. Labropoulos, B. Iliev, G. Adamova, T. Schubert, M. Kroon, M. Francisco, et al., Zeolite imidazolate framework–ionic liquid hybrid membranes for highly selective co2 separation, J. Phys. Chem. C 117 (2013) 18434–18440.
[39] Y. Ban, Z. Li, Y. Li, Y. Peng, H. Jin, W. Jiao, A. Guo, P. Wang, Q. Yang, C. Zhong, et al., Confinement of ionic liquids in nanocages: tailoring the molecular sieving properties of zif-8 for membrane-based co2 capture, Angew. Chem. Int. Ed. 54 (2015) 15483–15487.
[40] Y. Shen, R. Abedin, F.R. Hung, On the performance of confined deep eutectic solvents and ionic liquids for separations of carbon dioxide from methane: molecular dynamics simulations, Langmuir 35 (2019) 3658–3671.
[41] Y. Zeng, K. Li, Q. Zhu, J. Wang, Y. Cao, S. Lu, Capture of co2 in carbon nanotube bundles supported with room-temperature ionic liquids: a molecular simulation study, Chem. Eng. Sci. 192 (2018) 94–102.
[42] R.G. Pereira, V.O. Valente, R.M. de Souza, L.J.A. Siqueira, Understanding co2 absorption by an ammonium-based ionic liquid confined in porous carbon material under applied voltage, J. Mol. Liq. 366 (2022) 120227.
[43] F. Yan, Y. Guo, Z. Wang, L. Zhao, X. Zhang, Efficient separation of co2/ch4 by ionic liquids confined in graphene oxide: a molecular dynamics simulation, Sep. Purif. Technol. 289 (2022) 120736.
[44] J. Zhang, Q. Zhang, X. Li, S. Liu, Y. Ma, F. Shi, Y. Deng, Nanocomposites of ionic liquids confined in mesoporous silica gels: preparation, characterization and performance, Phys. Chem. Chem. Phys. 12 (2010) 1971–1981.
[45] Y. Tian, Y. Liu, H. Wang, L. Liu, W. Hu, Electrocatalytic reduction of nitrogen to ammonia in ionic liquids, ACS Sustain. Chem. Eng. 10 (2022) 4345–4358.
[46] F. Zhou, L.M. Azofra, M. Ali, M. Kar, A.N. Simonov, C. McDonnell-Worth, C. Sun, X. Zhang, D.R. MacFarlane, Electro-synthesis of ammonia from nitrogen at ambient temperature and pressure in ionic liquids, Energy Environ. Sci. 10 (2017) 2516–2520.
[47] W. Shi, D.R. Luebke, Enhanced gas absorption in the ionic liquid 1-n-hexyl-3-methylimidazolium bis (trifluoromethylsulfonyl) amide ([hmim][tf2n]) confined in silica slit pores: a molecular simulation study, Langmuir 29 (2013) 5563–5572.
[48] W. Shi, D.C. Sorescu, Molecular simulations of co2 and h2 sorption into ionic liquid 1-n-hexyl-3-methylimidazolium bis (trifluoromethylsulfonyl) amide ([hmim][tf2n]) confined in carbon nanotubes, J. Phys. Chem. B 114 (2010) 15029–15041.
[49] S. Tsuzuki, W. Shinoda, M.S. Miran, H. Kinoshita, T. Yasuda, M. Watanabe, Interactions in ion pairs of protic ionic liquids: comparison with aprotic ionic liquids, J. Chem. Phys. 139 (2013).
[50] W. Humphrey, A. Dalke, K. Schulten, Vmd: visual molecular dynamics, J. Mol. Graph. 14 (1996) 33–38.
[51] T.J. Vlugt, M. Schenk, Influence of framework flexibility on the adsorption properties of hydrocarbons in the zeolite silicalite, J. Phys. Chem. B 106 (2002) 12757–12763.
[52] J. Wang, Y. Zhu, J. Zhou, X.-H. Lu, Diameter and helicity effects on static properties of water molecules confined in carbon nanotubes, Phys. Chem. Chem. Phys. 6 (2004) 829–835.
[53] P. Kowalczyk, S. Furmaniak, P.A. Gauden, A.P. Terzyk, Optimal single-walled carbon nanotube vessels for short-term reversible storage of carbon dioxide at ambient temperatures, J. Phys. Chem. C 114 (2010) 21465–21473.
[54] H. Montes-Campos, T. Mendez-Morales, J.M. Otero-Mato, O. Cabeza, L.J. Gallego, E. Lomba, L.M. Varela, Ionic liquids nanoconfined in zeolite-templated carbon: a computational study, J. Mol. Liq. 318 (2020) 114264.
[55] W.L. Jorgensen, D.S. Maxwell, J. Tirado-Rives, Development and testing of the OPLS all-atom force field on conformational energetics and properties of organic liquids, J. Am. Chem. Soc. 118 (1996) 11225–11236.
[56] A. Rivera-Pousa, R. Lois-Cuns, M. Otero-Lema, H. Montes-Campos, T. Méndez-Morales, L.M. Varela, Size matters: a computational study of hydrogen absorption in ionic liquids, J. Chem. Inf. Model. 64 (2024) 164–177, https://doi.org/10.1021/acs.jcim.3c01688.
[57] J.J. Potoff, J.I. Siepmann, Vapor–liquid equilibria of mixtures containing alkanes, carbon dioxide, and nitrogen, AIChE J. 47 (2001) 1676–1682.
[58] M. Pérez-Rodríguez, J. Otero-Fernández, A. Comesaña, A.M. Fernández-Fernández, M.M. Piñeiro, Simulation of capture and release processes of hydrogen by β-hydroquinone clathrate, ACS Omega 3 (2018) 18771–18782.
[59] S. Plimpton, Fast parallel algorithms for short-range molecular dynamics, J. Comput. Phys. 117 (1995) 1–19.
[60] W.G. Hoover, Canonical dynamics: equilibrium phase-space distributions, Phys. Rev. A 31 (1985) 1695–1697.
[61] J.-P. Ryckaert, G. Ciccotti, H.J.C. Berendsen, Numerical integration of the Cartesian equations of motion of a system with constraints: molecular dynamics of n-alkanes, J. Comput. Phys. 23 (1977) 327–341.
[62] H. Bekker, H.J.C. Berendsen, E.J. Dijkstra, S. Achterop, R. van Drunen, D. van der Spoel, A. Sijbers, H. Keegstra, et al., Gromacs: a parallel computer for molecular dynamics simulations, Phys. Comput. 92 (1993) 252–256.
[63] D. van der Spoel, E. Lindahl, B. Hess, G. Groenhof, A.E. Mark, H.J.C. Berendsen, Gromacs: fast, flexible and free, J. Comput. Chem. 26 (2005) 1701–1718.
[64] M.J. Abraham, T. Murtola, R. Schulz, S. Páll, J. Smith, B. Hess, E. Lindahl, Gromacs: high performance molecular simulations through multi-level parallelism from laptops to supercomputers, SoftwareX 1 (2015) 19–25.
[65] G. Bussi, D. Donadio, M. Parrinello, Canonical sampling through velocity rescaling, J. Chem. Phys. 126 (2007) 014101.
[66] B. Hess, H. Bekker, H.J.C. Berendsen, J.G.E.M. Fraaije, Lincs: a linear constraint solver for molecular simulations, J. Comput. Chem. 18 (1997) 1463–1472.
[67] B. Hess, P-lincs: a parallel linear constraint solver for molecular simulation, J. Chem. Theory Comput. 4 (2007) 116–122.
[68] T. Darden, D. York, L. Pedersen, Particle mesh Ewald: an $n\,log(n)$ method for Ewald sums in large systems, J. Chem. Phys. 98 (1993) 10089–10094.
[69] A.v. Bondi, van der Waals volumes and radii, J. Phys. Chem. 68 (1964) 441–451.
[70] F. Borghi, A. Podestà, Ionic liquids under nanoscale confinement, Adv. Phys. X 5 (2020) 1736949.
[71] A.S. Pensado, F. Malberg, M.C. Gomes, A.A. Pádua, J. Fernández, B. Kirchner, Interactions and structure of ionic liquids on graphene and carbon nanotubes surfaces, RSC Adv. 4 (2014) 18017–18024.